Deep-Sea Research II 56 (2009) 161–172

Contents lists available at ScienceDirect

Deep-Sea Research II

journal homepage: www.elsevier.com/locate/dsr2

The correlation between surface drifters and coherent structures based on high-frequency radar data in Monterey Bay

Shawn C. Shadden [a,*], Francois Lekien [b], Jeffrey D. Paduan [c], Francisco P. Chavez [d], Jerrold E. Marsden [e]

[a] Bioengineering, Stanford University, Stanford, CA 94305, USA
[b] École Polytechnique, Université Libre de Bruxelles, B-1050 Brussels, Belgium
[c] Naval Postgraduate School, Monterey, CA 93943, USA
[d] Monterey Bay Aquarium Research Institute, Moss Landing, CA 95039, USA
[e] Control and Dynamical Systems, California Institute of Technology, Pasadena, CA 91125, USA

ARTICLE INFO

Article history:
Accepted 16 August 2008
Available online 26 September 2008

Keywords:
Lagrangian coherent structures
Aperiodic flows
Chaotic transport
Lyapunov exponents
Drifters
Coastal radar

ABSTRACT

This paper investigates the transport structure of surface currents around the Monterey Bay, CA region. Currents measured by radar stations around Monterey Bay indicate the presence of strong, spatial and temporal, nonlinear patterns. To understand the geometry of the flow in the bay, Lagrangian coherent structures (LCS) are computed. These structures are mobile separatrices that divide the flow into regions of qualitatively different dynamics. They provide direct information about the flow structure but are geometrically simpler than particle trajectories themselves. The LCS patterns were used to reveal the mesoscale flow conditions observed during the 2003 Autonomous Ocean Sampling Network (AOSN-II) experiment.

Drifter paths from the AOSN experiment were compared to the patterns induced by the LCS computed from high-frequency radar data. We verify that the fate of the drifters can be better characterized based on the LCS than direct interpretation of the current data. This property can be exploited to optimize drifter deployment.

© 2008 Elsevier Ltd. All rights reserved.

0. Introduction

Recent technological advances in ocean sensing, such as high-frequency radar technology, have allowed vast improvements in the measurement of surface currents. It is now possible to obtain high-resolution space–time measurements of the surface velocity fields in coastal regions, see Paduan and Rosenfeld (1996), Shay et al. (2002), Beckenbach and Washburn (2004) and Roughan et al. (2005). Analysis of this data often reveals many well-known *coherent structures* related to transport: major currents, vortex structures, upwellings, downwellings, squirts, etc. In general, coherent structures may be classified as spatially coherent patterns that are sufficiently persistent in time. While this definition is somewhat vague and only appropriate for a coarse understanding of the general dynamics, the definition of coherent structure used in this paper allows a more quantitative partitioning of the dynamics and helps unveil important Lagrangian flow features that are difficult to precisely capture with traditional analysis.

Measurements of the ocean's velocity field, $\mathbf{v}$, are entered into a data set that defines this field at discrete points in space and time. If we restrict the analysis to the ocean surface, then $\mathbf{v} = (u(x,y,t), v(x,y,t))$, where x and y denote spatial coordinates on the ocean surface, t denotes time, and u and v are the components of the velocity field in the x- and y-directions, respectively. The equations of motion of a fluid particle are given by

$$\begin{aligned} \dot{x} &= u(x,y,t) \\ \dot{y} &= v(x,y,t) \end{aligned} \tag{1}$$

Eq. (1) can be integrated numerically to answer a number of interesting questions. However, trajectories of such time-dependent systems are inherently chaotic and can change drastically with even small perturbations to the velocity field, such as errors in the measurement of $\mathbf{v}$. Therefore direct interpretation of particle trajectories can be difficult, if not misleading. Locating robust, coherent patterns that dictate transport, such as separatrices that partition the flow, is often more enlightening, as will be shown.

There have been recent developments to studying systems given by Eq. (1), even when the time variation is arbitrary and $\mathbf{v}$ is only known over a finite-time interval. The techniques are based

* Corresponding author.
E-mail address: sshadden@gmail.com (S.C. Shadden).

0967-0645/$ - see front matter © 2008 Elsevier Ltd. All rights reserved.
doi:10.1016/j.dsr2.2008.08.008

on the knowledge that transport is strongly influenced by *hyperbolicity* (Ottino, 1989). Hyperbolic structures in the flow are characterized by how particles behave in their vicinity. There are direction(s) of significant stretching along which fluid moves away from the structure and direction(s) of attraction where particles approach the structure. In the analysis of steady or periodic systems, hyperbolic stagnation points play a critical role. Such stagnation points have stable, and unstable, manifolds, which are composed of all trajectories that asymptote to the stagnation point in forward, and backward, time, respectively. These manifolds typically partition finite regions of qualitatively different dynamics. For time-periodic systems, these manifolds often interweave to provide a mechanism that stretches and folds parcels of fluid particles, which is the basis of chaotic transport (Guckenheimer and Holmes, 1986), and a number of analytic tools are available for analysis of such systems. For aperiodic systems, a complete theory of chaotic stirring does not yet exist. Nevertheless, similar stretching and elongation of fluid parcels are frequently observed, and there are often analogous "invariant manifolds" that organize the transport structure, which we refer to as Lagrangian coherent structures (LCS).

The most common methods for computing LCS in aperiodic systems involve either locating finite-time hyperbolic trajectories and growing their associated *finite-time invariant manifolds*, which in general are the LCS one seeks, or detecting these structures based on some local measure of hyperbolicity. Locating finite-time hyperbolic trajectories (Haller and Poje, 1998; Haller, 2000; Mancho et al., 2004) often assumes that the time-variation of the system is benign, and leads to conditions that are difficult to verify in many practical applications. Detecting LCS from measures of hyperbolicity has shown strong promise, even in turbulent flows, and includes measures such as hyperbolic time, finite-size Lyapunov exponents (FSLE), finite-strain, and finite-time Lyapunov exponents (FTLE). The hyperbolic-time approach (Haller and Yuan, 2000; Haller, 2001) measures the amount of time a trajectory *continuously* repels nearby trajectories. The FSLE is a measure of how quickly initially close particles reach a specified separation (Koh and Legras, 2002; Joseph and Legras, 2002). The finite-strain measure (Jones and Winkler, 2002) and the FTLE (Haller, 2001; Shadden et al., 2005) can be thought of as ways to measure the relative dispersion about a given trajectory over a finite-time interval. All of these methods take a similar approach but our experience has been that the FTLE offers one of the more convenient and robust methods for analysis of "raw" measurements of surface currents.

The setting for the analysis presented in this paper is the Autonomous Ocean Sampling Network (AOSN) experiment conducted in Monterey Bay, CA during late July through early September 2003, which is overviewed by Ramp et al. (2008). Although LCS have previously been computed in the context of studying ocean dynamics (e.g. Lekien et al., 2005), the goals of this paper are to show that LCS remain valid separatrices when the data are subject to large experimental errors, to relate the observed LCS patterns to the mesoscale conditions observed in the Monterey Bay region during the AOSN experiment, and to introduce a new drifter deployment strategy that improves coverage and recovery effort.

1. Coastal radar measurements

The surface current mapping data used in this study were derived from a network of four *CODAR SeaSonde* high-frequency radar systems deployed around the shores of Monterey Bay. In a clockwise direction, the first system is near Santa Cruz, the second system at Moss Landing, the third system at the *Naval Postgraduate School of Monterey*, and the fourth system at Point Pinos (see Fig. 1 for locations). The systems operate on frequencies between 12 and 25 MHz, producing estimates of the radial current speeds approaching or receding from the radar sites based on hourly averaged ocean backscatter. The angular resolution of the radial data produced by a single radar site is 5° and the range resolution is 3 km. Single-component, radial current data from individual sites were combined for regions of overlapping coverage to estimate the vector surface current patterns each hour. This allowed estimations of vector currents in the region of overlap, which extended 40–50 km offshore. No additional temporal smoothing was done for the results presented herein. Therefore, significant high frequency (diurnal and semi-diurnal period) fluctuations driven by tides and sea breeze wind forcing are present in the data set, as have been reported on elsewhere for the Monterey Bay region (Paduan and Rosenfeld, 1996; Paduan and Cook, 1997; Rosenfeld et al., 2008).

The results in this paper were obtained using "raw" recombined velocity field measurements. Our objective is to avoid effects from filtering and smoothing to show that computations derived directly from the raw HF radar data renders the fundamental coherent structures governing the transport of drifters.

The range resolution of the individual systems was 3 km and vector current estimates were produced, where possible, on a Cartesian grid every 2.5 km by fitting radial observations within a radius of 3 km from each grid point. The nature of the direction-finding mapping approach used by the *CODAR SeaSonde* HF radar systems is such that individual, hourly radial current maps for a given radar site contain spatial gaps in the coverage. These gaps result from system limitations during times of weak current speeds as well as from azimuthal pointing errors (Paduan et al., 2006; dePaolo and Terrill, 2007). The coverage was very good in the interior of the bay but worsened outside the bay and near the coastline (Fig. 1). For the present analysis, any gaps in the HF radar measurements had to be filled. To keep processing minimal, missing data points are linearly interpolated based on surrounding data in space and time.

Errors in the individual surface velocity estimates derive from a number of sources. The study of error sources and propagation in HF radar-derived surface current estimates is underway on a number of fronts, including further comparison against *in situ*

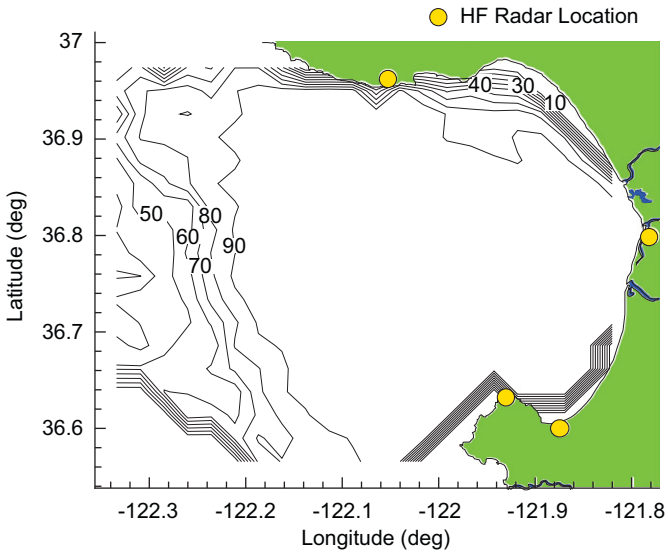

Fig. 1. Percent coverage of the velocity field data derived from HF radar measurements for August 12 to August 29, 2003.

mooring and drifter observations (Paduan and Rosenfeld, 1996; Paduan et al., 2006; Ohlmann et al., 2007) and theoretical simulation studies (e.g. Laws et al., 2000). The effective depth of currents measured from any HF radar system is a weighted function of the particle motions exhibited by the Bragg-resonant surface wave constituent (Paduan and Graber, 1997). In the case of the Monterey Bay HF radar network, the Bragg-resonant wavelengths were between 3 and 6 m, which implies effective measurement depths between 25 and 50 cm using the rule-of-thumb estimate of 8% of the wavelength (Stewart and Joy, 1974).

2. Lagrangian coherent structures

Here we use the FTLE to located LCS. High FTLE values indicate high stretching between fluid trajectories. In two-dimensional (surface) flows, there are typically well-defined curves of high FTLE, such as shown in Fig. 2. Curves of high FTLE appear as *ridges* in the graph of the FTLE field and serve as the mathematical definition of LCS (Shadden et al., 2005).

To compute the FTLE, the right-hand side of Eq. (1) is integrated to provide the *flow map*, $\phi_t^T : \mathbf{x}(t) \mapsto \mathbf{x}(t+T)$, which maps fluid particles from their initial location at time t to their location after some interval of time T. The symmetric matrix

$$S(\mathbf{x}, t; T) = \left(\frac{\mathrm{d}\phi_t^T(\mathbf{x})}{\mathrm{d}\mathbf{x}}\right)^{\top} \frac{\mathrm{d}\phi_t^T(\mathbf{x})}{\mathrm{d}\mathbf{x}} \tag{2}$$

(where the $A^{\top}$ denotes the transpose of the matrix A) is a finite-time version of the (right) Cauchy–Green deformation tensor. Letting $\lambda_{\max}(S)$ denote the largest eigenvalue of S,

$$\sigma(\mathbf{x}, t; T) = \frac{1}{|T|} \ln \sqrt{\lambda_{\max}(S)} \tag{3}$$

represents the FTLE at the location $\mathbf{x}$ at time t with an integration time T. The FTLE is the time-averaged maximum exponential stretching about the trajectory of $\mathbf{x}(t)$.

The FTLE field is computed from the following steps: first, a two-dimensional structured grid was generated to discretize the computation of the FTLE field. The span of this grid coincides with the span of the velocity data, however, the spatial resolution is 10 times the resolution of the velocity data. Points in the FTLE grid are treated as fluid particles and advected by numerically integrating the HF radar velocity data. For example, to produce Fig. 2 an integration length of $T = 96$ h is used. The deformation tensor was then computed over the grid by finite-differencing the trajectories. The FTLE is obtained over the grid from straightforward evaluation of Eq. (3). The time variation of the FTLE field can be computed by following the previous steps, but varying the evaluation time, t.

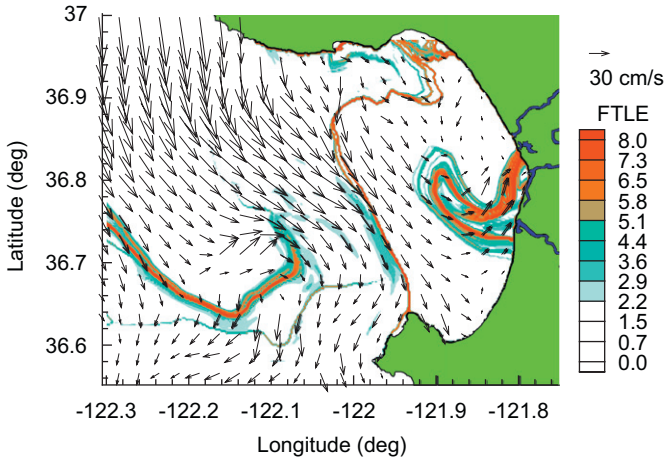

Fig. 2. FTLE field computed from HF radar velocity data. Curves of high FTLE represent time-varying LCS. Also shown is HF radar velocity field at the given time.

LCS are typically attached to some boundary or dychotomic point in the flow (a "hyperbolic trajectory"), which itself can be unsteady. If $T > 0$ in the computation of the FTLE, then the LCS are *repelling*. Trajectories on opposite side of a repelling LCS typically move along the LCS then become exponentially stretched by the hyperbolic trajectory. These LCS reveal the global effect of these hyperbolic trajectories, which are influential in a wide range of flows. Knowing the location of the LCS, one can better understand the time-dependent global flow structure, and thus understand the geometry of many interesting transport driven processes. For oceanographic applications, LCS have been used in pollution release studies (Lekien et al., 2005), optimal trajectory generation of gliders in the ocean (Inanc et al., 2005), and predicting scalar fronts and algal blooms (Olascoaga et al., 2006). Additionally, LCS often reveal many interesting phenomena such as large-scale eddies, squirts, upwellings, etc. (Bhatta et al., 2005; Beron-Vera et al., 2008). The exact geometry of such flow features is often vague from quantities directly derived from Eulerian velocity fields, since such fields only represent snapshots of the unsteady flow. When $T < 0$, ridges in the FTLE field are referred to as attracting LCS. These LCS are also very useful for studying transport, but are not considered in this study.

The length of the integration time $|T|$ is flexible. The LCS typically become better resolved the longer the integration length. However, the location of the LCS, which is tantamount, is in general not sensitive to variations of the integration length used to compute the FTLE field. Since most points in the FTLE grid are advected outside the HF radar domain within a couple of days, extending the integration length T beyond 3–4 days does not change the FTLE field much. This is because once a point leaves the HF radar domain through the open boundary, the integration must cease and FTLE is computed for that point based on the available trajectory information.

The computation of the FTLE requires the advection of particle grids. Such advection was achieved by a tricubic interpolation scheme (Lekien et al., 2005) along with a Runge–Kutta–Fehlberg integration method (Fehlberg, 1969). Therefore, between grid points, the data are interpolated, which smooths out subgrid-scale turbulence. From a spectral point of view, turbulent velocity fluctuations are truncated at $2\pi/2.5$ km in space and $2\pi/1$ h in time. The measurement of the velocity data also filters small-scale turbulence. As we will show in the remainder of this paper, the LCS computed for the radar data (neglecting small-scale turbulence) are remarkably accurate for describing and predicting the motion of ocean drifter (whose paths in the ocean are subject to the entire turbulent spectrum). This need not be the case in general, however. In fully established three-dimensional turbulent flows, the $k^{-5/3}$ energy spectrum induces much larger velocity gradients at small scales than at the macroscopic scales. In such a system, the FTLE is mostly governed by small-scale fluctuations and surface radar data are unlikely to induce the correct LCS. In Monterey Bay, however, the flow is quasi-turbulent and the energy behaves as k^{-3}, a much steeper decrease. As a result, the dominant velocity gradient and LCS are found at the largest scales (Lekien and Coulliette, 2007). As shown in the next sections, the match between the LCS and the paths of ocean drifters is evidence that the small-scale portion of the energy spectrum does not significantly modify the motion of drifters in Monterey Bay, at least over the timescales studied.

As previously mentioned, LCS act as separatrices that divide dynamically distinct regions. In this sense it should be a necessary condition that these structures are transport barriers. Shadden

et al. (2005) derive estimates that show that for sufficiently well-defined LCS, these structures can indeed be considered transport barriers. In most practical applications, as for all the LCS shown herein, the flux through the LCS is negligible. We stress, however, that it is their separatrix behavior that is of greatest value when trying to understand geometrically how the fluid is behaving.

For example, the LCS that extends across the mouth of the bay in Fig. 2 divides the flow that re-circulates within the bay from the flow that moves down the California coast. Fig. 3(A) shows the LCS, extracted from the FTLE field on August 14, 2003, 00:00 GMT and an arbitrary grid of fluid particles, where particles to the right of the LCS are denoted by empty circles, and those to the left of the LCS are shaded. Panels (B)–(D) shows the time evolution of these particles along with the time evolution of the LCS. The shaded particles are shown to move down the California coast and exit the domain, while the unshaded particles remain inside the LCS and recirculate within the bay. Without knowledge of the LCS, it would be very difficult to easily infer the extent of the recirculation. This re-attachment point that oscillates around the Monterey Peninsula has been studied further by Lekien and Haller (2008).

In addition to the smoothing of sub-gridscale turbulence mentioned above, measured data always contains some deviation from the physical system. Furthermore, small errors in the velocity field measurement typically result in large integrated errors on particle trajectories. However, LCS depict hyperbolic regions in the flow. Hyperbolic structures are usually robust to perturbations of the governing dynamics. Haller (2002) showed that the LCS can be robust to oscillating perturbations, even with significant amplitudes. Although specific knowledge of errors is not available for the hourly surface current maps used in this study, an uncertainty level of, approximately, 10 cm/s for the radar-derived velocity components is supported by a wide number of previous studies (Paduan and Rosenfeld, 1996; Paduan et al., 2006; Ohlmann et al., 2007). In addition it has been observed that the majority of the noise has a sub-tidal variability. This is quite a substantial noise level but the comparison in Section 5 between data collected from drifter experiments and LCS computed from the HF radar data demonstrate that the computation of LCS tends to mitigate this error.

3. Drifters

To compare the LCS computed from HF radar data with observed surface advection patterns, we use drifting buoy data measured during the AOSN-II field experiment. The drifting buoy position data were obtained from deployments of a set of GPS-tracked surface drifters, Fig. 4. The instruments included a cylindrical surface float approximately 1 m across that supported a holey sock-style drogue element approximately 8 m long centered around 5.5 m depth (Paduan et al., 2006).

Estimates of the drift characteristics of this particular buoy suggest a drag area ratio around 20 and slip or error currents in the range 1–3 cm/s for winds under 10 m/s (Niiler and Paduan, 1995). The physical drifter design was a compromise between optimal water following characteristics near the surface and support for additional bio-chemical sensors.

Deployments were made at locations estimated to be upstream of the majority of field observations in place around Monterey Bay in order to maximize the time individual drifters stayed in the region. In practice, this meant deploying along the northwest

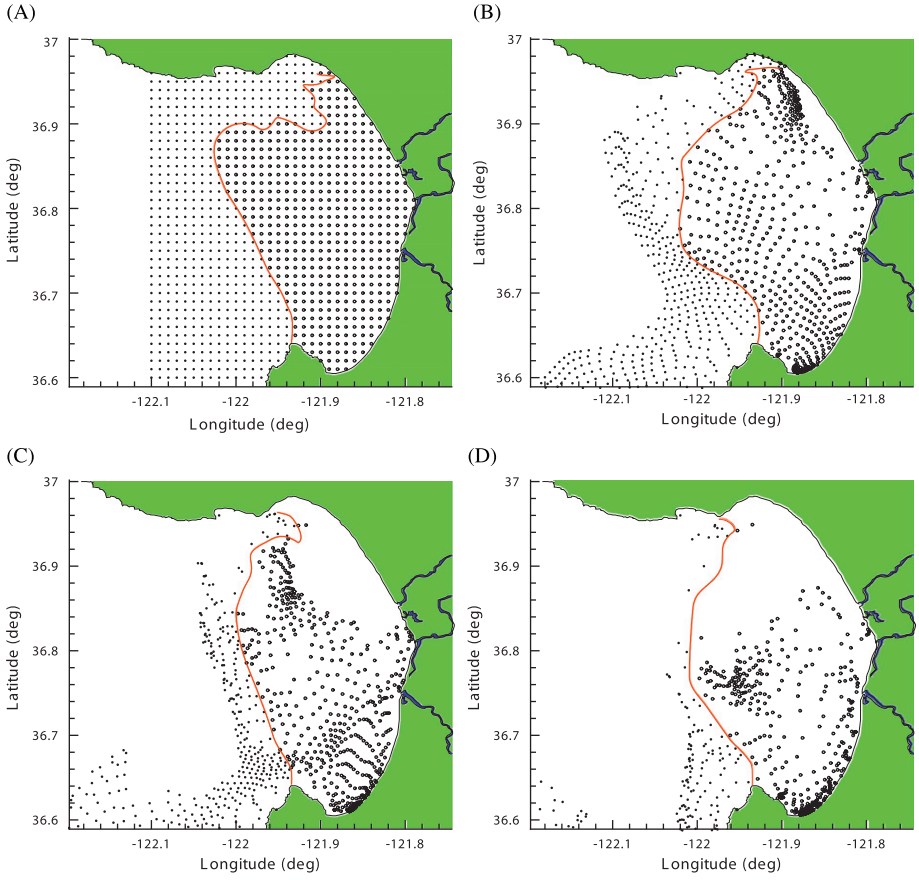

Fig. 3. The LCS that extends across the mouth of the bay is a moving separatrix, dividing fluid that recirculates in the bay from fluid that moves down the California coast.

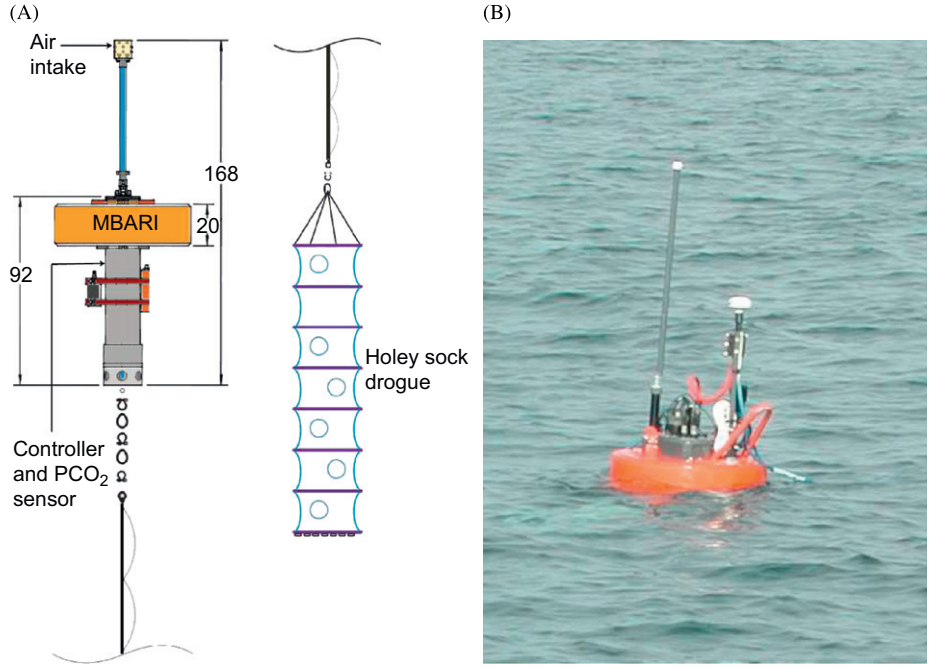

Fig. 4. A schematic (A) and the physical drifters (B) that are used to compare the drifter paths with LCS computed from HF radar data. Lengths are in cm.

Table 1
Drifter release and recovery times and positions

Drifter	Release	Recovery
A	8/11 08:00 (−122.220, 36.890)	8/13 00:00 (−122.061, 36.554)
	8/13 15:00 (−122.136, 36.923)	8/15 01:00 (−122.087, 36.556)
	8/16 15:00 (−121.980, 36.795)	8/18 17:00 (−121.865, 36.690)
B	8/11 21:00 (−121.918, 36.798)	8/12 22:00 (−121.822, 36.679)
	8/13 23:00 (−121.903, 36.795)	8/15 14:00 (−121.865, 36.715)
	8/17 01:00 (−122.011, 36.893)	8/18 17:00 (−121.910, 36.719)
	8/19 14:00 (−121.951, 36.902)	8/21 16:00 (−122.225, 36.846)
	8/21 21:00 (−121.981, 36.839)	8/29 15:00 (−121.881, 36.744)
C	8/14 23:00 (−121.914, 36.917)	8/17 16:00 (−121.950, 36.717)
	8/19 14:00 (−121.953, 36.902)	8/21 16:00 (−122.230, 36.846)
	8/21 21:00 (−121.982, 36.768)	8/25 16:00 (−121.923, 36.668)
	8/25 22:00 (−121.932, 36.922)	8/29 03:00 (−121.934, 36.641)
D	8/23 00:00 (−121.922, 36.858)	8/29 14:00 (−121.842, 36.795)

Times are listed in GMT and position in decimal degrees longitude and latitude.

portion of Monterey Bay and recovery further south or inside the bay. Since the biogeochemical sensors on the drifters were being tested for the first time, the locations that allowed for easy recovery were chosen. Also there was an interest in knowing the general circulation within Monterey Bay during the period and in particular if there were two standing eddies, one in the north bay and a second in the south bay. These factors all influenced the general release strategy. The exact locations and times for the deployment and recovery of each drifter used in the field experiment are given in Table 1.

4. Upwelling and relaxation

The results in this paper span data collected during the month of August 2003. During this period, the Monterey Bay region experienced distinct upwelling and relaxation phases. Upwelling is characterized by a southward-flowing filament of cold, salty water that rises from just north of the bay and spreads southward. A prominent cause of the upwelling is strong northwesterly winds (Ramp et al., 2005). The winds were consistently upwelling-favorable from around August 6 to August 18. During August 18–22, the winds briefly calmed and reversed to a more south-westerly direction, resulting in a *relaxation* state in the bay. This caused the upwelling to disappear and resulted in an onshore flow in the southern portion of the bay, which generally allows warmer water to spread into the bay from the south. The winds switched back to upwelling-favorable toward the end of August. Stick plots of the winds during this time-frame are shown in Fig. 5 at two moorings located in the bay.

During the upwelling stage, there is typically an LCS that extends across the mouth of the bay. As mentioned in Section 2, this LCS separates the fluid that recirculates inside the bay from fluid that moves down the California coast. Thus, upwelling appears to be responsible for producing recirculation of the surface fluid inside the bay. This observation is also consistent with LCS computations on HF radar data from an upwelling period during August 2000, which produced an analogous LCS across the mouth of the bay. Therefore, we consider this LCS as a *Lagrangian footprint* of ongoing upwelling in the bay.

Around August 18, the upwelling-favorable winds calmed and reversed direction. This created relaxation-favorable conditions. During transition to relaxation, the LCS extending from Point Pinos pushed southward, offshore, and eventually disappeared by the end of August 19. As shown in Fig. 8(A), there was a well-defined LCS that stretched into the northern section of the bay that curved back and forth tracing out "lobes" of fluid. The transfer of fluid via lobes was first studied in the context of perturbed Hamiltonian systems (Ottino, 1989) but has recently been noticed in more general systems (e.g. Coulliette and Wiggins, 2000; Koh and Legras, 2002; Shadden et al., 2006, 2007). Water in the northern region of the bay was transported offshore via lobes enclosed by the LCS, as shown in Fig. 8. Subsequently, the LCS moved further up the coast, pushing an influx of water in the

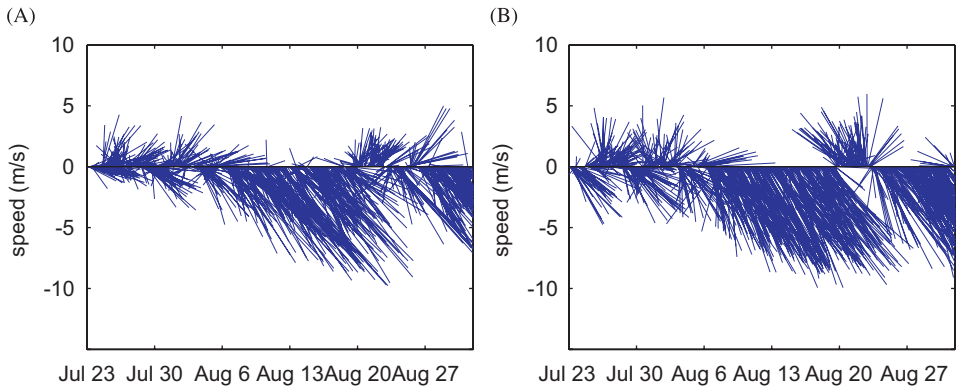

Fig. 5. Direction from which wind blows from August 23, 2003 to September 1, 2003, measured at moorings M1 (36.75 N, −122.03 W) and M2 (36.70 N, −122.39 W) (Chavez, 2006). North is the upward direction. (A) M1 winds, (B) M2 winds.

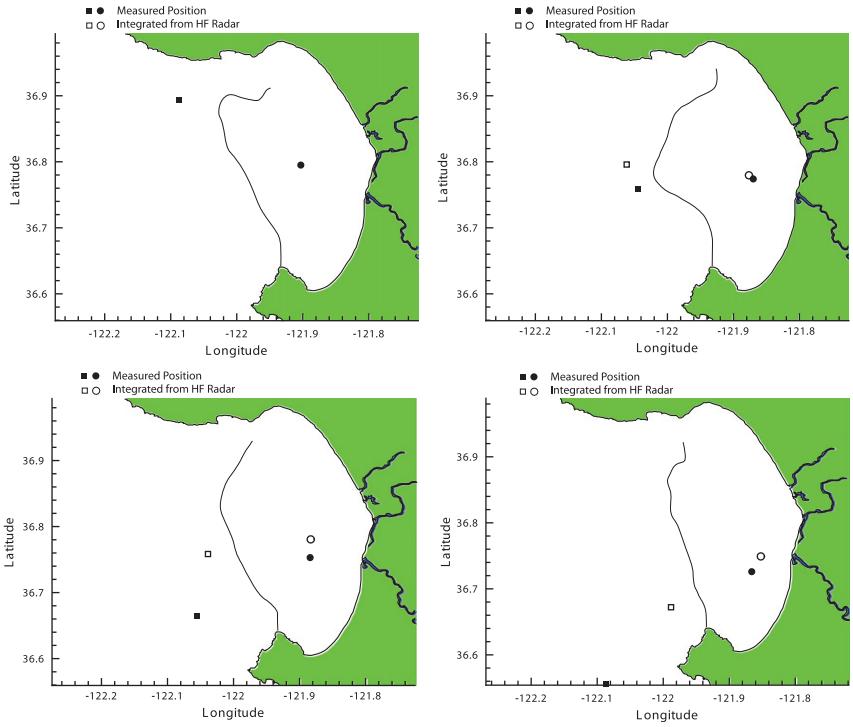

Fig. 6. Time series locations of drifter A (square) and drifter B (circle) during their second releases superimposed with an LCS.

lower portion of the bay during the days of August 20–23. Such flow structure is consistent with the dynamics typically associated with relaxation.

Toward the end of August, the winds switched back to upwelling-favorable. After a brief transient period of a couple days, a well-defined LCS extending off Point Pinos developed (cf. Fig. 7), which is analogous to the LCS observed during the August 6–18 upwelling stage, reaffirming that this LCS is a footprint of upwelling.

5. Comparison of LCS with drifters

The purpose of this section is to compare the paths of the drifters deployed during AOSN-II with the LCS computed from HF radar observations to understand how robust the LCS are to predicting the advection of surface drifting buoys. One question that can be asked is whether a drifter starting on one side of an LCS stays confined by the LCS. For example, if a drifter starts inside the LCS that spans across the bay during upwelling, does it stay in the bay? Or alternatively, if it starts outside the LCS, does it get advected down the coast? Or better yet, if two drifters straddle an LCS, are the ultimate fates of the two drifters distinctly different? The interest is not so much whether the LCS represents a transport barrier, but rather how close the computed LCS is to its true location; the separatrix property of LCS is what makes these structures interesting.

Fig. 6 shows snapshots of two GPS-tracked drifters, laconically named A and B, during their second releases, along with the time evolution of an LCS computed from HF radar. The wind-forcing was upwelling favorable and there was a well-defined LCS attached near Point Pinos that extended across the mouth of the bay. Also shown are the predicted locations of drifters A and B obtained by integrating the HF radar data. The two drifters straddle either side of the LCS. Drifter A remains outside the bay and moves down the California coast while drifter B remains

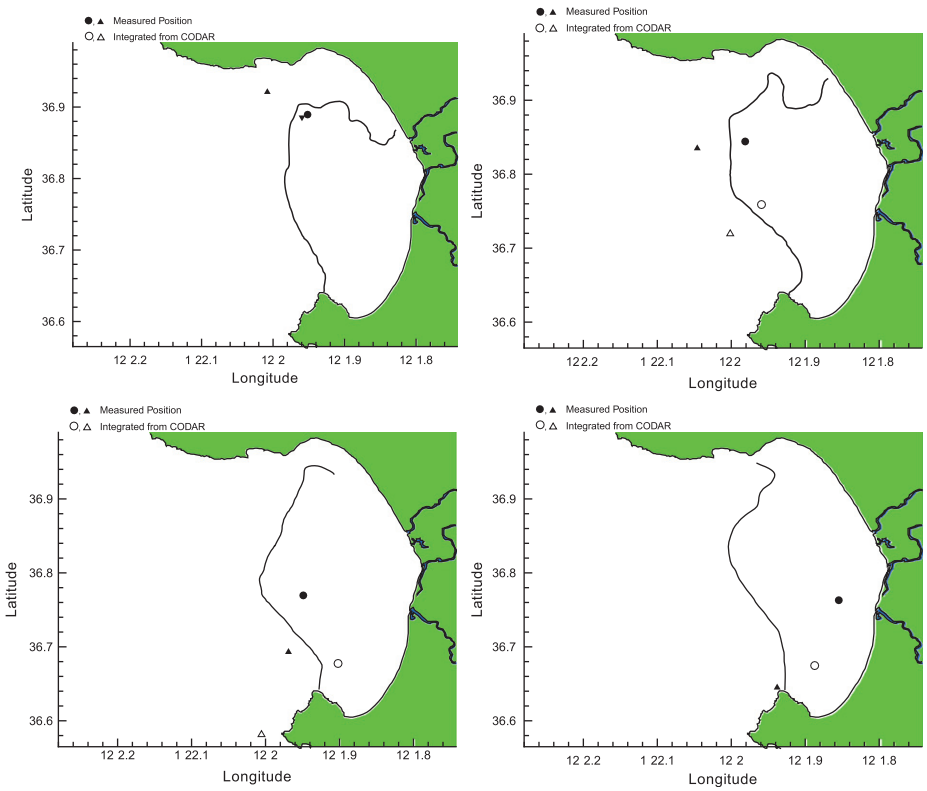

Fig. 7. Time series locations of drifters B (circle) and C (triangle) superimposed with an LCS.

inside the bay. The dynamics of the drifters are consistent with the expected dynamics based solely on knowledge of the LCS; drifters outside the LCS will move down the California coast and drifters inside will recirculate. Although the initial separation of the drifters does not provide a tight bound on the error in the position of the LCS, it is clear, at least heuristically, that the error in the location of the LCS is significantly less than the error between measured and computed paths of drifters, which can reach more than a 15 km discrepancy in just one day, such as for drifter A.

On August 26, during the second period of upwelling-favorable conditions, drifters B and C were released in proximity to the LCS extending across the mouth of the bay, as shown in Fig. 7. These deployments allowed a better estimate of the error between the true location of the LCS and the computed location based on the HF radar observations. The two drifters diverge, with the inner drifter re-circulating and the outer drifter moving down the coast; therefore it is reasonable to assume that the true location of the LCS is transversed by the segment connecting the two drifters. Since the initial separation between the drifters is about 4.5 km, the local error in the position of the LCS is less then 4.5 km. Again, notice that the error in the location between the drifting buoy and the location predicted by integrating the HF radar data reaches almost 14 km in just over a day. The LCS has far less error, even though it was computed from integrating $T = 3$ days of HF radar data, confirming that errors in the velocity data cause significant deviations in the computed paths of drifters, but relatively small deviations in the location of the LCS even though it is based on trajectory information.

The LCS are computed from HF radar data while the drifters are GPS-tracked devices that are, at least approximately, transported by the true currents. The agreement between the drifter paths and the motion of the LCS supports that, first, although the flow in Monterey Bay is quasi-turbulent (k^{-3} energy spectrum), the large-scale features measured by HF radar are the most relevant in determining drifter paths; and second, since there exists large discrepancies between drifter paths integrated from radar data and actual drifter paths, the LCS computations are robust such errors.

The change in wind shear around August 18 forced relaxation-favorable conditions that greatly changed the flow geometry of the surface currents. This is also apparent in the Lagrangian dynamics by inspection of the LCS during this time frame. The LCS across the mouth of the bay is no longer present. However, there is an LCS in the northern bay that loops back and forth enclosing lobes of fluid. The fourth deployment of drifter B placed it in one of these lobes as shown in Fig. 8(A). The subsequent panels show that the drifter was transported off-shore following a path consistent with the dynamics predicted by the LCS.

The paths of the drifters shown in Figs. 6 and 7 straddle the LCS and thus help provide a bound on the error of the LCS location, while Fig. 8 helps demonstrate the interesting change in dynamics associated with relaxation. Since the deployment of the drifters was not coordinated with computations of LCS, not all drifter data were useful in determining the sensitivity of the LCS to errors in the velocity measurements. However, for completeness Fig. 9 plots the "signed distance" between each drifter that was deployed during the AOSN-II experiment and the closest point on the relevant LCS. The sign of the distance was set according to the side of the LCS the drifter was on. As with Figs. 6–8, the relevant LCS was chosen to be the one closest to the drifter after the deployment. Since the distance between a drifter and an LCS is directly proportional to determining a bound on the error in the location of the LCS, the drifters determined which LCS could be analyzed, as opposed to first choosing an LCS then deploying drifters. There were typically only 2–3 LCS in the HF radar domain at any given time during the drifter experiments that were sufficiently defined, which meant that, with the exception of the

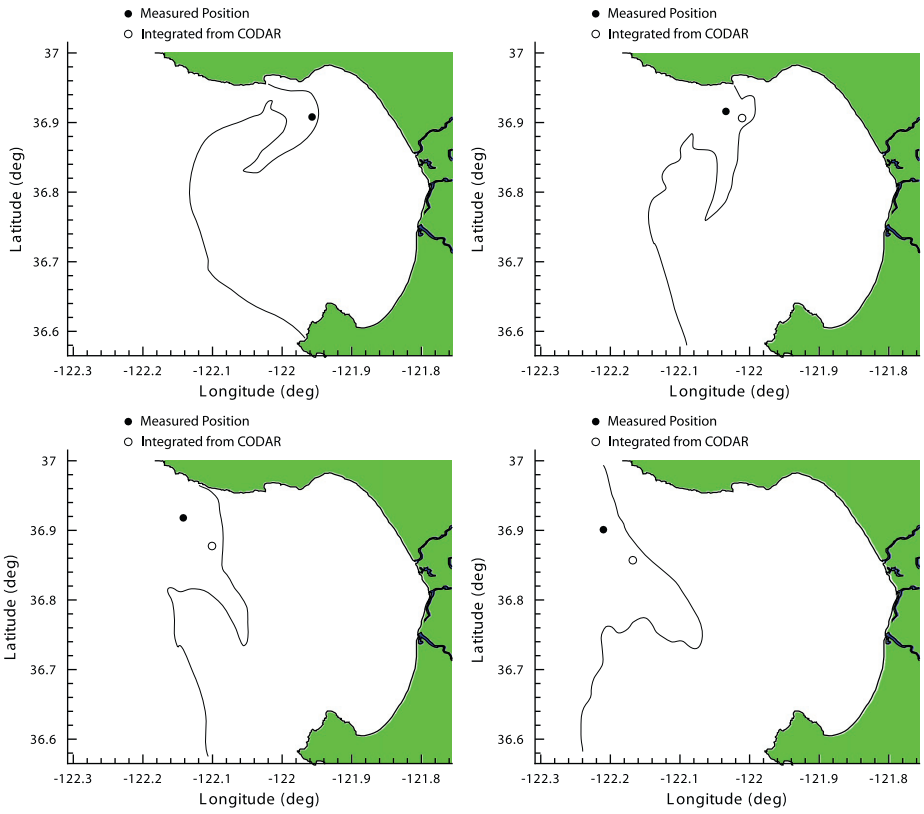

Fig. 8. Time series locations of drifter B superimposed with an LCS during relaxation.

third watertime for drifter C, there was never ambiguity of the relevant LCS to use to compare with each drifter path. Data from deployment 2 for drifter C and deployment 1 for drifter D are not plotted in Fig. 9 as they are not significantly different than the data from deployments 4 and 5 for drifter B.

Although some information is lost when condensing the spatial relation between the drifter paths and the dynamics of the LCS to a single graph, the results shown in Fig. 9 demonstrate that the drifter paths are generally consistent with the LCS. However, inspection of Fig. 9 reveals that there is indeed error in the location of the LCS computed from HF radar data. The first deployment of drifter C and the third and fifth deployments of drifter B cross the LCS. These crossings only occurred when the deployment of the drifter was less than 2 km from the location of the LCS. This indicates that the computation of the LCS has around a 2 km spatial error in location. This error is significantly less than typical error between measured and computed drifter paths, which can easily reach deviations commensurate to the overall length of the domain within the time frame used to computed the FTLE fields.

6. Optimal drifter release

A possible application of LCS is to assist tasks such as drifter deployment. Drifters are common to coastal observatory systems, providing Lagrangian measures of the currents and, depending on their sensor payload, measurements such as temperature, salinity, fluorescence, nitrate, and scattering (Abbott et al., 1995; Niiler and Paduan, 1995). Drifters passively follow the ocean currents, thus planning effective release and recovery strategies can be difficult without proper understanding of the ocean dynamics. Poje et al. (2002) proposed a release strategy that places drifters at the base of *attracting* LCS to maximize dispersion. This technique appears promising for regions where there the fluid continues to mix for a long time. For coastal regions, such as Monterey Bay, the fluid is not in general confined to the domain and the LCS move rapidly so that a release strategy similar to Poje et al. (2002) requires frequent and costly recoveries. In this section, we demonstrate how *repelling* LCS can be used to improve drifter use.

The LCS shown in Fig. 10 was obtained from the FTLE field on July 23, 2003, 18:00 GMT computed from HF radar data. We will demonstrate a numerical (hypothetical) study to show that releasing drifters based on knowledge of the LCS can keep the drifters in the bay significantly longer than typical deployments, reducing the need for frequent recovery. The lighter-shaded group is located on the side of the LCS facing the shore and the darker-shaded group is placed on the other side. Fig. 11 shows that the darker-shaded group remains relatively close together, and exits the domain of interest within about 5.5 days (thus necessitating recovery) whereas members of the lighter-shaded group remain in the bay up to 16 days, nearly 3 times longer. When a drifter comes sufficiently close to the coastline, it is removed, i.e., considered recovered.

The significant expense of deployment and recovery motivates keeping the drifters autonomous for as long as possible. But it is important to also consider each group's ability to measure the ocean. To quantify the measurement capability of each group of drifters, optimal interpolation (Leonard et al., 2007; Rudnick et al., 2004) is considered. Optimal interpolation is used to assimilate measurements to provide an updated estimate of the field being measured and an estimate of the uncertainty. This technique, based on objective analysis (Eliassen et al., 1954; Gandin, 1963), provides a metric that quantifies the coverage of the measurements in both space and time. In particular, the residual error in optimal interpolation is based on the spatial coverage of the measurements and the decorrelation of measurements in time.

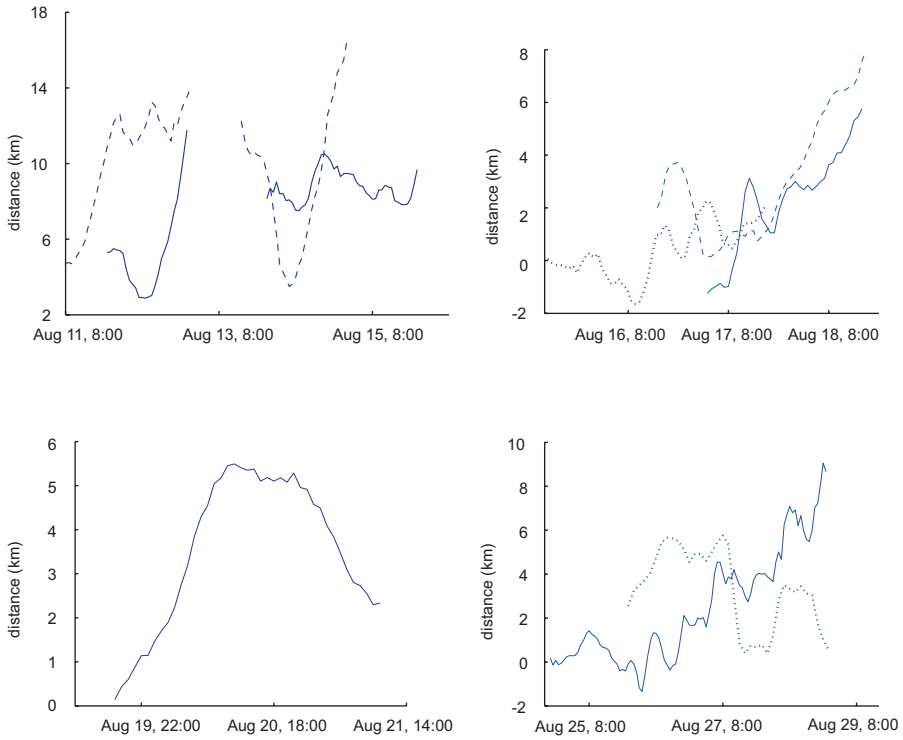

Fig. 9. Time history of signed distance between drifting buoys and LCS. Drifter A: dashed line, drifter B: solid line, drifter C: dotted line.

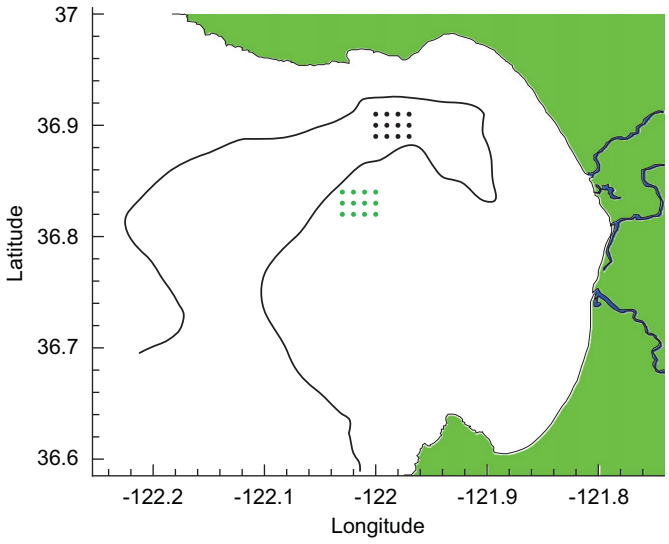

Fig. 10. Panel (A) shows the location of an LCS on 07-23-2003, 18:00 GMT. Panel (B) shows the initial locations of two arrays of drifters on either side of the LCS.

The objective analysis metric for each group (the logarithm of the inverse residual sampling error) is given in Fig. 12. The information from the darkly shaded drifters (solid curve) becomes insignificant after four or five days. The drifters have left the domain and the only information available is historical data that decays at a decorrelation rate of two days (Rudnick et al., 2004). On the other hand, the dashed curve (lightly shaded drifters) indicates that valuable information is collected for almost 13 days.

Without integrating specific drifter paths, it would be difficult to predict which drifters might remain in the bay. One would likely guess that those located further inside the bay or placed further north would obtain better coverage of the domain, but Fig. 11 shows that this is not necessarily the case. Even if estimated drifter paths are computed from computational or empirical data, these paths are highly sensitive to errors in the data. Recent work (Lipphardt et al., 2006) shows that, even for highly filtered and smoothed data, the escape time of drifters is highly sensitive to the initial release location. This is even more apparent when we look at unfiltered data and realistic flows. LCS provide a geometric framework that let us understand and predict the complexity of the trajectories observed in Lipphardt et al. (2006). Knowing the location of the LCS, allows quick assessment where to drop drifters such that they have the desired dynamics.

Some practical concerns are worth mentioning. Even though the LCS is a moving separatrix, we only have to know the location of the LCS at the time when the drifter is released. There is no need to continually compute the LCS. Although we require future information about the surface currents to compute the LCS at the release time, this does not present an insurmountable obstacle. The integration time, T, used to compute the LCS shown in Fig. 10 was three days. However, ocean models are currently capable of making reliable predictions of the ocean dynamics within this time window. Since the location of LCS is relatively robust to uncertainty in the velocity field, we might expect a reliable estimate of the LCS location from moderately uncertain current data. Alternatively, the movements of LCS are typically much slower than the average fluid particle dynamics, since on average the flow is tangential to these structures. Therefore it is reasonable to assume that time-lagged locations of LCS computed from observational data could be used in certain circumstances for real-time applications (Coulliette et al., 2007).

Although the integration time used to compute the LCS shown in Fig. 10 was three days, this, remarkably, allowed us to keep the drifters inside the bay for up to 16 days. This can be attributed to the robustness of the LCS. Although one cannot guarantee that the drifters will remain in the bay much longer than the integration time of the LCS, we expect the LCS to persist much longer than the integration time length. Thus, if we were to take the naive approach of directly

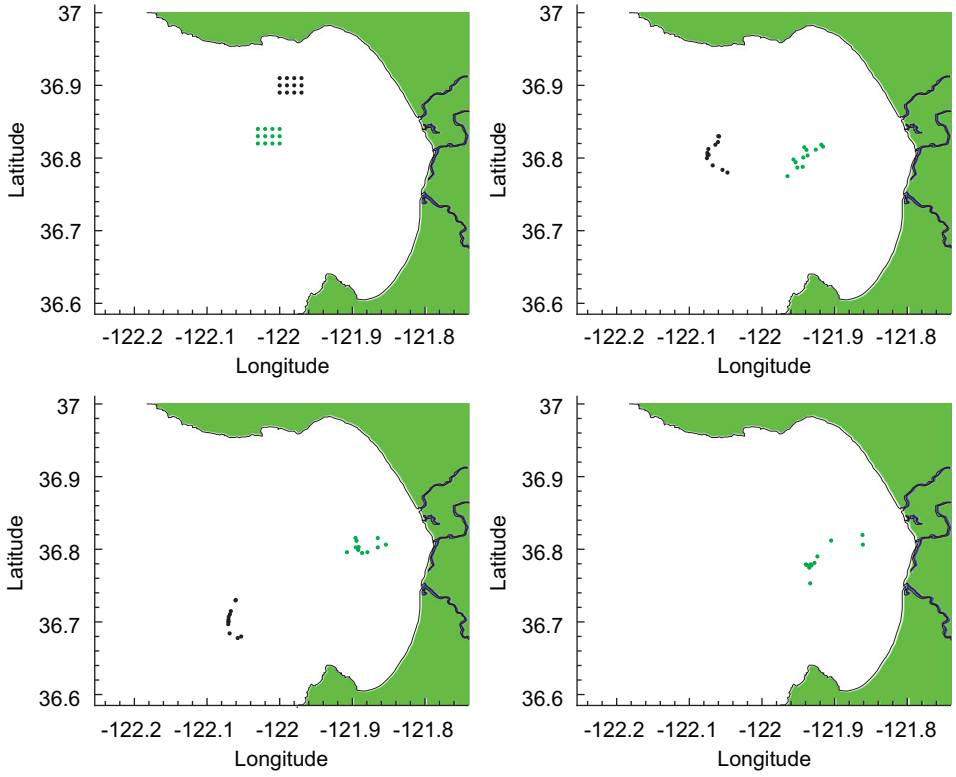

Fig. 11. Time series location of the two groups of drifters release on either side of the LCS shown in Fig. 10.

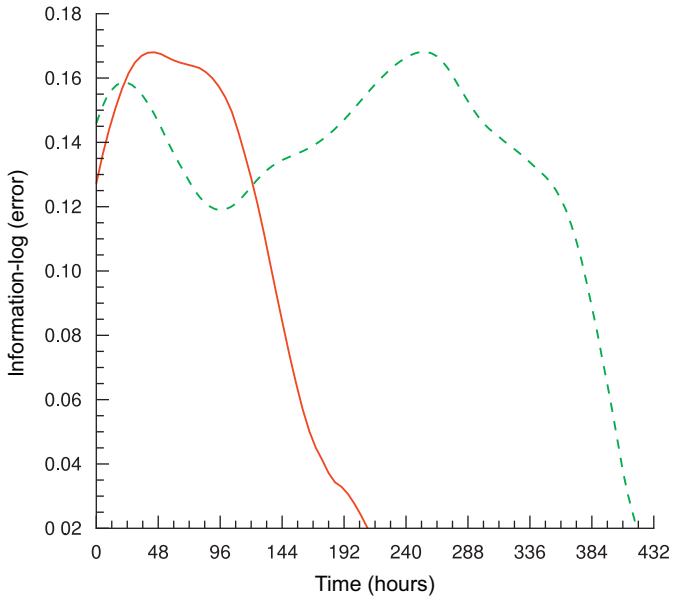

Fig. 12. Objective analysis metric for the two groups of drifters in Fig. 11.

investigating trajectories computed from ocean model predictions, we would require a much longer prediction time, which is unrealistic. Furthermore, individual trajectories are subject to the "butterfly effect," making them highly sensitive to errors in the velocity data, whereas the locations of LCS are much more robust to such errors.

7. Discussion and conclusions

Real fluid flows are usually unsteady and often quasi-turbulent, making it difficult to understand transport by inspection of the velocity field. While the velocity data can be integrated to provide individual particle trajectories, these trajectories are usually complicated and highly sensitive to errors in velocity field measurements. However, more structured, frame-independent techniques are being developed to reveal the underlying structure that dictates the complicated stirring patterns observed in unsteady and turbulent systems. This paper has presented the application of such a technique to surface currents in Monterey Bay during the AOSN-II experiment.

Velocity fields were obtain from HF radar measurements of the surface currents in and around the bay. These data were numerically integrated to provide FTLE fields, and hence LCS. It was shown in Section 5 that even if drifter trajectories integrated from the HF radar significantly deviate from measured drifter paths, the LCS computed from integrating HF radar data are robust indicators of separatrices in the actual flow. These results confirm that this method is robust to noise and perturbations of the velocity field, which confirms previous analytical results (Haller, 2002).

A case study was presented to demonstrate that LCS can be used to plan effective release strategies for drifters used for ocean measurement. By releasing drifters based on the location of repelling LCS, the amount of time the drifters can be kept in the domain of the experiment was increased by nearly threefold, minimizing frequent recovery.

During the AOSN experiment, there was a strong upwelling-favorable period from August 6 up to August 18. Also during this period, there was a consistently well-defined LCS that extended across the mouth of the bay. This observation is consistent with observations of the upwelling period during the first AOSN in August 2000 that produced an analogous LCS across the mouth of the bay. This LCS is likely a footprint that the bay is experiencing upwelling. Around August 18, the upwelling-favorable winds reversed direction, creating relaxation-favorable conditions. During this transition to relaxation, the LCS extending off Point Pinos,

moved further down shore, and eventually disappeared, allowing an influx of water in the lower portion of the bay during August 20–22, which is consistent with dynamics typically associated with relaxation.

The drifters available in this study used a relatively long drogue element and were, therefore, not optimized for validation of 1 m deep HF radar-derived surface current products. HF radar observations measure current footprints at the ocean surface, which can have variations from the dynamics a few meters below depending on the local flow conditions. This discrepancy can introduce errors, in addition to inherent measurement uncertainty, when comparing the drifter paths with those predicted by HF radar measurement (Paduan and Cook, 1997). Paduan et al. (2006) report differences between HF radar-derived radial current estimates and drifter-derived velocity components in the direction of the radar site for the data set used in this analysis. At least part of the reported velocity differences can be attributed to vertical shear. This contributes to the differences between the integrated drifter trajectories and the measured trajectories shown in Figs. 6–8, although the relative influence of this is questionable. However, even though there are large deviations in these trajectories, both sets were relatively consistent with the LCS. Work is currently underway to obtain trajectories of surface drifters that follow more closely the surface ocean dynamics, and use that data to compare with the LCS computed from HF radar. Such a comparison would help factor out the inherent discrepancies in dynamics caused by the vertical variation of the flow and help focus on the robustness of LCS to measurement errors in the velocity data.

Conceptually, the LCS method discussed in this paper is not restricted to surface flows (Lekien et al., 2007) and current work is underway to study LCS, not just at the surface, but for the full three-dimensional ocean dynamics. This could test whether there is a well-defined two-dimensional LCS (surface embedded in the full three-dimensional ocean) that can be associated with the upwelling plume, which results from the upwelling-favorable wind forcing. If so, such a geometry could greatly aid in the visualization and subsequent interpretation of this upwelling phenomenon, and other inherently three-dimensional flow structures. Additionally, true upwelling should cause divergence in the surface velocity field. Divergence may cause areas of stretching (sources) or compression (sinks). These may show up as regions of high FTLE instead of well-defined LCS. Although prior FTLE computations from HF radar observations yield well-defined LCS and not typically regions of stretching, the LCS perspective is not appropriate for flows with significant divergence. Extending the computation to three-dimensional would circumvent the "artificial" divergence introduced by considering only the surface currents.

Acknowledgments

The research in this paper was supported in part by the ASAP MURI project, ONR-MURI Contract N00014-04-1-0534.

References

Abbott, M.R., Brink, K.H., Booth, C.R., Blasco, D., Swenson, M.S., Davis, C.O., Codispoti, L.A., 1995. Scales of variability of bio-optical properties as observed from near-surface drifters. Journal of Geophysical Research 100, 13345–13368.

Beckenbach, E., Washburn, L., 2004. Low-frequency waves in the Santa Barbara channel observed by high-frequency radar. Journal of Geophysical Research—Oceans 109 (C02), C020101–C020118.

Beron-Vera, F.J., Olascoaga, M.J., Goni, G.J., 2008. Oceanic mesoscale eddies as revealed by Lagrangian coherent structures. Geophysical Research Letters 35 (12).

Bhatta, P., Fiorelli, E., Lekien, F., Leonard, N.E., Paley, D.A., Zhang, F., Bachmayer, R., Davis, R.E., Fratantoni, D., Sepulchre, R., 2005. Coordination of an underwater fleet for adaptive sampling. In: International Workshop on Underwater Robotics, pp. 61–69.

Chavez, F., 2006. M1 and M2 mooring hydrography and meteorology data, Autonomous Ocean Sampling Network (AOSN) 2003 field experiment. Retrieved April 25, 2006, from ⟨http://aosn.mbari.org⟩.

Coulliette, C., Wiggins, S., 2000. Intergyre transport in a wind-driven, quasigeostrophic double gyre: an application of lobe dynamics. Nonlinear Processes in Geophysics 7 (1–2), 59–85.

Coulliette, C., Lekien, F., Haller, G., Paduan, J., Marsden, J.E., 2007. Optimal pollution mitigation in Monterey Bay based on coastal radar data and nonlinear dynamics. Environmental Science and Technology 41 (18), 6562–6572.

dePaolo, T., Terrill, E., 2007. Skill assessment of resolving ocean surface current structure using compact-antenna style HF radar and the MUSIC direction finding algorithm. Journal of Atmospheric and Oceanic Technology 24 (7), 1277–1300.

Eliassen, A., Sawyer, J.S., Smagorinsky, J., 1954. Upper air network requirements for numerical weather prediction. Technical Note of the World Meteorological Organization 29.

Fehlberg, E., 1969. Low-order classical runge-kutta formulas with step size control and their application to some heat transfer problems. NASA Technical Report 315.

Gandin, L.S., 1963. Gidrometerologicheskoe Izdatelstvo—Objective Analysis of Meteorological Fields. English Translation by Israeli Program for Scientific Translations, Leningrad, Jerusalem.

Guckenheimer, J., Holmes, P., 1986. Nonlinear Oscillations, Dynamical Systems, and Bifurcations of Vector Fields. Applied Mathematical Sciences. Springer, New York.

Haller, G., 2000. Finding finite-time invariant manifolds in two-dimensional velocity fields. Chaos 10 (1), 99–108.

Haller, G., 2001. Distinguished material surfaces and coherent structures in three-dimensional fluid flows. Physica D 149 (4), 248–277.

Haller, G., 2002. Lagrangian coherent structures from approximate velocity data. Physics of Fluids 14 (6), 1851–1861.

Haller, G., Poje, A.C., 1998. Finite time transport in aperiodic flows. Physica D—Nonlinear Phenomena 119 (3–4), 352–380.

Haller, G., Yuan, G., 2000. Lagrangian coherent structures and mixing in two-dimensional turbulence. Physica D—Nonlinear Phenomena 147 (3–4), 352–370.

Inanc, T., Shadden, S.C., Marsden, J., 2005. Optimal trajectory generation in ocean flows. In: American Control Conference, Portland, OR, USA, pp. 674–679.

Jones, C.K.R.T., Winkler, S., 2002. Invariant manifolds and Lagrangian dynamics in the ocean and atmosphere. In: Fiedler, B. (Ed.), Handbook of Dynamical Systems, vol. 2. Elsevier, Amsterdam, pp. 55–92.

Joseph, B., Legras, B., 2002. Relation between kinematic boundaries, stirring, and barriers for the Antarctic polar vortex. Journal of the Atmospheric Sciences 59 (7), 1198–1212.

Koh, T.Y., Legras, B., 2002. Hyperbolic lines and the stratospheric polar vortex. Chaos 12 (2), 382–394.

Laws, K., Fernandez, D., Paduan, J., 2000. Simulation-based evaluations of HF radar ocean current algorithms. Journal of Oceanic Engineering 25, 481–491.

Lekien, F., Coulliette, C., 2007. Chaotic stirring in quasi-turbulent flows. Philosophical Transactions of the Royal Society A 365 (1861), 3061–3084.

Lekien, F., Haller, G., 2008. Unsteady flow separation on slip boundaries. Physics of Fluids 20.

Lekien, F., Coulliette, C., Mariano, A.J., Ryan, E.H., Shay, L.K., Haller, G., Marsden, J., 2005. Pollution release tied to invariant manifolds: a case study for the coast of Florida. Physica D—Nonlinear Phenomena 210 (1–2), 1–20.

Lekien, F., Shadden, S.C., Marsden, J.E., 2007. Lagrangian coherent structures in n-dimensional systems. Journal of Mathematical Physics 48 (6), 065404.

Leonard, N.E., Paley, D.A., Lekien, F., Sepulchre, R., Fratantoni, M., Davis, R.E., 2007. Collective motion, sensor networks and ocean sampling. In: Proceedings of the IEEE, Special Issue on Networked Control Systems, vol. 95, pp. 48–74.

Lipphardt, B.L., Small, D., Kirwan, A.D., Wiggins, S., Ide, K., Grosch, C.E., Paduan, J.D., 2006. Synoptic Lagrangian maps: application to surface transport in Monterey Bay. Journal of Marine Research 64 (2), 221–247.

Mancho, A.M., Small, D., Wiggins, S., 2004. Computation of hyperbolic trajectories and their stable and unstable manifolds for oceanographic flows represented as data sets. Nonlinear Processes in Geophysics 11 (1), 17–33.

Niiler, P.P., Paduan, J.D., 1995. Wind-driven motions in the Northeast Pacific as measured by Lagrangian drifters. Journal of Physical Oceanography 25 (11), 2819–2830.

Ohlmann, J., White, P., Washburn, L., Terrill, E., Emery, B., Otero, M., 2007. Interpretation of coastal HF radar derived surface currents with high resolution drifter data. Journal of Atmospheric and Oceanic Technology 24 (4), 666–680.

Olascoaga, M.J., Rypina, I.I., Brown, M.G., Beron-Vera, F.J., Kocak, H., Brand, L.E., Halliwell, G.R., Shay, L.K., 2006. Persistent transport barrier on the West Florida Shelf. Geophysical Research Letters 33 (22).

Ottino, J.M., 1989. The Kinematics of Mixing: Stretching, Chaos, and Transport. Cambridge Texts in Applied Mathematics. Cambridge University Press, New York.

Paduan, J.D., Cook, M.S., 1997. Mapping surface currents in Monterey Bay with CODAR-type HF radar. Oceanography 10, 49–52.

Paduan, J.D., Graber, H.C., 1997. Introduction to high frequency radar: reality and myth. Oceanography 10, 36–39.

Paduan, J.D., Rosenfeld, L.K., 1996. Remotely sensed surface currents in Monterey Bay from shore-based HF radar (coastal ocean dynamics application radar). Journal of Geophysical Research—Oceans 101 (C9), 20669–20686.

Paduan, J.D., Kim, H.C., Cook, M.S., Chavez, F., 2006. Calibration and validation of direction-finding high frequency radar ocean surface current observations. IEEE Journal of Oceanic Engineering 31, 862–875.

Poje, A.C., Toner, M., Kirwan, A.D., Jones, C.K.R.T., 2002. Drifter launch strategies based on Lagrangian templates. Journal of Physical Oceanography 32 (6), 1855–1869.

Ramp, S.R., Paduan, J.D., Shulman, I., Kindle, J., Bahr, F.L., Chavez, F., 2005. Observations of upwelling and relaxation events in the Northern Monterey Bay during August 2000. Journal of Geophysical Research-Oceans 110 (C7), C07013.

Ramp, S.R., Davis, R.E., Leonard, N.E., Shulman, I., Chao, Y., Robinson, A.R., Marsden, J., Lermusiaux, P., Fratantoni, D., Paduan, J.D., Chavez, F., Bahr, F.L., Liang, S., Leslie, W., Li, Z., 2008. Preparing to predict: the second Autonomous Ocean Sampling Network (AOSN-II) experiment in the Monterey Bay. Deep-Sea Research II, this issue [doi:10.1016/j.dsr2.2008.08.013].

Rosenfeld, L., Shulman, I., Cook, M., Paduan, J., Shulman, L., 2008. Methodology for a regional tidal model evaluation, with application to central California. Deep-Sea Research II, this issue [doi:10.1016/j.dsr2.2008.08.007].

Roughan, M., Terrill, E.J., Largier, J.L., Otero, M.P., 2005. Observations of divergence and upwelling around Point Loma, California. Journal of Geophysical Research—Oceans 110 (C4).

Rudnick, D.L., Davis, R.E., Eriksen, C.C., Fratantoni, D.M., Perry, M.J., 2004. Underwater gliders for ocean research. Marine Technology Society Journal 38 (1), 48–59.

Shadden, S.C., Lekien, F., Marsden, J.E., 2005. Definition and properties of Lagrangian coherent structures from finite-time Lyapunov exponents in two-dimensional aperiodic flows. Physica D—Nonlinear Phenomena 212 (3–4), 271–304.

Shadden, S.C., Dabiri, J.O., Marsden, J.E., 2006. Lagrangian analysis of fluid transport in empirical vortex rings. Physics of Fluids 18, 047105.

Shadden, S.C., Katija, K., Rosenfeld, M., Marsden, J.E., Dabiri, J.O., 2007. Transport and stirring induced by vortex formation. Journal of Fluid Mechanics 593, 315–331.

Shay, L.K., Cook, T.M., Peters, H., Mariano, A.J., Weisberg, R., An, E., Soloviev, A., Luther, M., 2002. Very high-frequency radar mapping of surface currents. IEEE Journal of Oceanic Engineering 27 (2), 155–169.

Stewart, R.H., Joy, J.W., 1974. HF radio measurements of surface currents. Deep-Sea Research 21 (12), 1039–1049.